Glioma-derived CCL2 and CCL7 mediate migration of immune suppressive CCR2$^+$ myeloid cells into the tumor microenvironment in a redundant manner

Gregory P. Takacs[1†], Christian J. Kreiger[1†], Defang Luo[1], Guimei Tian[2], Julia S. Garcia[1], Loic P. Deleyrolle[2], Duane A. Mitchell[2], and Jeffrey K. Harrison[1*]

[1]Department of Pharmacology & Therapeutics, University of Florida College of Medicine, Gainesville, FL, USA

[2]Department of Neurosurgery, University of Florida College of Medicine, Gainesville, FL, USA

*** Correspondence:**
Jeffrey K. Harrison
jharriso@ufl.edu

[†]These authors have contributed equally to this work and share first authorship

Keywords: Glioma, Chemokine, Chemokine Receptor, Migration, Immune-suppression, Myeloid, MDSC, Bone Marrow

Abstract

Glioblastoma (GBM) is the most common and malignant primary brain tumor, resulting in poor survival despite aggressive therapies. GBM is characterized in part by a highly heterogeneous and immunosuppressive tumor microenvironment (TME) made up predominantly of infiltrating peripheral immune cells. One significant immune cell that contributes to glioma immune evasion is a population of immunosuppressive, hematopoietic cells, termed myeloid-derived suppressor cells (MDSCs). Previous studies suggest that a potent subset of myeloid cells, expressing monocytic(M)-MDSC marker, distinguished by dual expression of chemokine receptors CCR2 and CX3CR1, utilize CCR2 to infiltrate into the TME. This study evaluated the T cell suppressive function and migratory properties of CCR2$^+$/CX3CR1$^+$ MDSCs. Bone marrow-derived CCR2$^+$/CX3CR1$^+$ cells adopt an immune suppressive cell phenotype when cultured with glioma derived factors. Recombinant and glioma-derived CCL2 and CCL7 induce the migration of CCR2$^+$/CX3CR1$^+$ MDSCs with similar efficacy. KR158B-CCL2 and -CCL7 knockdown murine gliomas contain equivalent percentages of CCR2$^+$/CX3CR1$^+$ MDSCs compared to KR158B gliomas. Combined neutralization of CCL2 and CCL7 completely blocks CCR2-expressing cell migration to KR158B cell conditioned media. High levels of CCL2 and CCL7 are also associated with negative prognostic outcomes in GBM patients. These data provide a more comprehensive understanding of the function of CCR2$^+$/CX3CR1$^+$ MDSCs and the role of CCL2 and CCL7 in the recruitment of these immune-suppressive cells and further support the significance of targeting this chemokine axis in GBM.

Introduction

Glioblastoma (GBM) is a highly aggressive and recurrent primary brain tumor that continues to challenge patients and oncologists as current interventions are minimally effective (1,2). Currently, standard of care therapy relies on surgical resection of the tumor mass followed by focal radiation and chemotherapy (temozolomide) (3–5). Foremost in GBM patients, the immune-suppressive tumor-microenvironment contributes to immune evasion, disease progression, and poor overall survival (6–9). Attempts at harnessing anti-tumor immune responses to overcome the immunosuppressive microenvironment have been made in cancer therapy (10–12). For example, clinically successful immunotherapy has targeted immune checkpoint systems, including the programmed cell death protein-1, i.e., PD-L1/PD-1, pathway. Unfortunately, to date targeting the PD-L1/PD-1 axis in human gliomas has not demonstrated efficacy as an adjuvant monotherapy (13,14). While the mechanism by which gliomas are resistant to PD-1 blockade is not entirely resolved, mounting evidence suggests that infiltrating immune-suppressive cells contribute significantly to the resistant phenotype (15–17).

Chief amongst the immune-suppressive cells which gain access to the glioma microenvironment are a subset of myeloid cells termed myeloid-derived suppressor cells (MDSCs) (15). In humans, MDSCs represent a heterogeneous cell population that are delineated into three major classes based on phenotypic and morphological features: early-stage (e), polymorphonuclear (PMN/G)-, and monocytic (M)-MDSCs (18,19). Although M-MDSCs are present within the human glioma microenvironment in a lower proportion than are the other subtypes, M-MDSCs display the most potent immune-suppressive phenotype through deleterious anti-tumor lymphocyte interactions. M-MDSCs suppress lymphocytes via production of free radicals and enzymes that deplete essential lymphocyte metabolites (20–23). In murine gliomas, M-MDSCs are the predominant subtype and are characterized by lineage markers CD45$^+$, CD11b$^+$, Ly6C^{hi}, and Ly6G$^-$ (19,24,25).

We have previously reported that three populations of myeloid cells are identified in the glioma microenvironment according to their expression of chemokine receptors CCR2 and CX3CR1. One of these populations, co-expressing chemokine receptors CCR2 and CX3CR1 (denoted as CCR2$^+$/CX3CR1$^+$), express markers consistent with M-MDSCs. Pharmacologic or genetic targeting of CCR2-expressing cells via a CCR2 antagonist or gene deletion limited the presence of these cells within the tumor and promoted their sequestration within the bone marrow. In combination with the immune checkpoint inhibitor, αPD-1, CCR2 antagonism unmasked an effect of PD-1 blockade in slowing the tumor progression of two immune checkpoint inhibitor-resistant murine gliomas (KR158B and 005 GSC) (26). While these previous findings established that CCR2$^+$/CX3CR1$^+$ MDSCs utilize CCR2 to traffic into the glioma microenvironment, it is unclear what chemokines drive this CCR2-dependent migration. This study investigated the T cell suppressive function and chemokine ligand dependency by which CCR2$^+$/CX3CR1$^+$ M-MDSCs traffic into the glioma microenvironment. Using a preclinical glioma model, we demonstrate that CCR2$^+$/CX3CR1$^+$ cells are sourced from the bone marrow, suppress both CD4 and CD8 T cells, and migrate to CCL2 and/or CCL7 in a CCR2 dependent manner. We also identify CCL2 and CCL7 as predictors of survival in human glioblastoma. These data establish the immune suppressive and migratory properties of CCR2$^+$/CX3CR1$^+$ myeloid cells and confirm their role as glioma-associated M-MDSCs.

Methods

Animals

Ccr2$^{RFP/WT}$/*Cx3cr1*$^{GFP/WT}$ mice were generated through the breeding of Ccr2-deficient (*Ccr2*$^{RFP/RFP}$*[B6.129(Cg)-Ccr2*$^{tm2.1Ifc}$*/J*]), and Cx3cr1-deficient (*Cx3cr1*$^{GFP/GFP}$*[B6.129P-Cx3cr1*^{tm1Litt}*/J*]) mice. Wildtype C57BL/6, Ccr2-deficient, and Cx3cr1-deficient mice were purchased from The Jackson Laboratory. All procedures involving animal housing and surgical protocols were followed according to the guidelines of the University of Florida Institutional Animal Care and Use Committee.

Generation of Chimeric Mice

Chimeric mice were generated through a bone marrow transplant of *Ccr2*$^{WT/RFP}$/*Cx3cr1*$^{WT/GFP}$ donor mice into wildtype C57BL/6 recipient mice. Wildtype mice were placed under anesthesia (Xylazine 0.5mL, Ketamine 0.7mL, Saline 5.6mL) through intra peritoneal injection (100µL/20g mouse). Subsequently, wildtype mice received 900 cGy x-ray radiation (X-RAD 350 irradiator). Bone marrow was prepared from *Ccr2*$^{WT/RFP}$/*Cx3cr1*$^{WT/GFP}$ mice as described below. Cells were diluted to a final concentration of 10,000 cells/µL. After irradiation (~4hrs), whole bone marrow from *Ccr2*$^{WT/RFP}$/*Cx3cr1*$^{WT/GFP}$ donor mice was tail vein injected (100 µL) into irradiated wildtype C57BL/6 recipient mice. Seven days post-irradiation, Baytril (fluoroquinolone antibiotic) was added to the drinking water was administered, 0.5 mg/ml for two weeks. Following recovery, chimeric mice were implanted with KR158B gliomas (see "Orthotopic Brain Tumor Model") and evaluated via flow cytometry (see "Flow Cytometry Analysis")

Orthotopic Brain Tumor Model

Animals were anesthetized using isoflurane and administered analgesia prior to cell injection. While under anesthesia, the surgical site was prepared, a 2- to 3-mm incision was made at the midline of the skull. Using a stereotaxic apparatus (Stoelting), the mice were secured, and a Hamilton syringe was positioned 2-mm lateral from the bregma. KR158B, KR158B-CCL2 knockdown, or KR158B-CCL7 glioma cells (3.5×10^4 in a total volume of 2 µL) were injected 3-mm deep into the right cerebral hemisphere using an automated microfluidic injection system (Stoelting) at a rate of 1 µL /min; cells were suspended in a 1:1 ratio of methylcellulose to PBS. Post injection, the needle was retracted slowly, and the surgical site was closed via suture and bone wax. Animals were then placed into a warm cage for postsurgical monitoring.

Tissue Isolation

Mice were euthanized at experimental endpoint. Transcardial perfusions, using a 10mL syringe with a 25G winged infusion set, of 20mL 0.9% saline solution were administered to remove intra-vasculature associated cells. Femurs, tibiae, and humeri were harvested from the animal. Fat and muscle were trimmed from the bones and were subsequently cut at one end to expose bone marrow. Bones were placed in microcentrifuge tubes (2 bones per tube) with the bottoms pierced and nested in 1.5mL centrifuge tubes containing 100uL PBS. Tubes were centrifuged at 5,700 x g for 20 seconds to flush the bone marrow. Spleens were harvested and placed on a petri dish. Fat was trimmed from the tissue and spleens were injected with 1mL PBS via 18G needle. Spleens were minced using a razor blade and transferred to 15mL conical tubes containing 5mL PBS. Using a 5mL syringe and 18G needle, the tissue was mechanically dissociated via passage through the needle 20 times. Splenocytes were collected via centrifugation (4 °C, 380 × *g*, 5 min). Bone marrow cells and

splenocytes were resuspended in 1mL Ammonium-Chloride-Potassium (ACK) Lysis buffer (Gibco, Invitrogen) and placed on ice for 5 min to lyse red blood cells. Subsequently, lysis buffer was quenched with 5mL fluorescence-activated cell-sorter (FACS) washing buffer (1% FBS in PBS) and strained through a 40-µm cell strainer. Cells were collected via centrifugation (4 °C, 380 × *g*, 5 min) and counted by trypan blue exclusion. Brains were removed and tumors were extracted and mechanically minced using a razor blade. Tumors were placed in 4 °C Accumax dissociation solution (Innovative Cell Technologies) and incubated at 37 °C for 5 min, followed by 5 min of agitation at room temperature. Cells were then passed through a 40-µm strainer, centrifuged (4 °C, 380 × *g*, 5 min), and resuspended in 4 mL of 70% Percoll (70% Percoll and 1% PBS in RPMI-1640 cell medium). The 70% Percoll/cell solution was then carefully layered beneath 37% Percoll layer (4 mL, 37% Percoll and 1% PBS in RPMI-1640 cell medium) using an 18-gauge needle. Samples were then centrifuged for 30min at room temperature (500 x g). Cells at the interface were collected and transferred into a 1.5 mL microcentrifuge tube. Cells were washed with cold PBS and counted by trypan blue exclusion.

Flow Cytometry Analysis

Single cell suspensions were prepared from tissues as described above and diluted to 1 x 10^6 cells/100uL. Subsequently, cells were stained for markers of interest (see Supplement Table 1) for 30 min at 4 °C. Cells were then washed twice in ice-cold PBS and stained with a viability dye. Stained samples were analyzed using single-color compensation on a Sony SP6800 spectral analyzer or Beckman Coulter CytoFLEX LX 96-well plate system and quantified using FlowJo V10.8.1 (BD Biosciences).

Cell Culture

KR158B, KR158B-Luciferase, KR158B-CCL2 knockdown, and KR158B-CCL7 knockdown glioma cells were cultured in Dulbecco's Modified Eagle Medium (DMEM) supplemented with 1% penicillin-streptomycin and 10% fetal bovine serum (FBS). Cells were grown in a humidified incubator at 37 °C with 5% CO_2. DMEM and penicillin-streptomycin were purchased through Invitrogen. FBS was purchased through Thermo Scientific.

Generation of CCL2 and CCL7 Deficient Glioma Cells

Plasmids for knockdown of CCL2 (TRCN0000301701 and TRCN0000301702) and CCL7 (TRCN0000317599, TRCN0000068135, and TRCN0000068136) were obtained from Sigma. shRNA control plasmid (SHC002. Sigma) was used as non-targeting control. ShRNA plasmids were purified with QIAprep Spin Miniprep Kit (#27106, Qiagen) after overnight incubation with E-coli bacteria. Packaging 293T/17 cells were co-transfected with the different shRNAs and the packaging plasmids psPAX2 and pMD2.G, to generate viral particles, which were subsequently used to transduce KR158B cells. KR158B-CCL2 knockdown were generated using the combination of TRCN0000301701 and TRCN0000301702. TRCN0000317599, TRCN0000068135, and TRCN0000068136 were combined to generate KR158B-CCL7 knockdown.

Cytokine Quantification

Cytokine quantification was completed using mouse CCL2 (Invitrogen# 88-7391-22) and mouse CCL7 (Invitrogen# BMS6006INST) enzyme linked immunosorbent assay (ELISA) analysis following manufacturer protocols. KR158B, KR158B-CCL2 knockdown and KR158B-CCL7 knockdown glioma cell lines were cultured to 90% confluency. Cells were counted and plated in a

156 96-well plate at 50, 100 or 500 cells/uL in 200uL complete DMEM media. Cells were incubated at
157 37°C, 5% CO_2 for 24 hours. Following incubation, cell contents were transferred to tubes and
158 centrifuged as previously described. Supernatant was aliquoted and frozen at -80°C until use for
159 ELISA as previously described.

160 **Mouse Brain Fixation and Immunohistochemistry**

161 Transcardial perfusions, using a 10mL syringe with a 25G winged infusion set, of 20mL 4.0%
162 paraformaldehyde (PFA) solution were administered. Following fixative perfusion, mouse brains
163 were removed and soaked in 4.0% PFA for 1hr. Brains were subsequently transferred to 30% sucrose
164 solution for 24hrs and snap frozen using liquid nitrogen chilled 2-Methylbutane. Brains were
165 embedded in optimal cutting temperature compound and mounted for cryo-sectioning (Lecia
166 Biosystems Cryostat). 5-10µm thick sections were taken and mounted on microscope slides. Sections
167 were dried overnight at 4°C. Tissue sections were brought to room-temperature and washed 3 times
168 in PBS and counter stained with antifade mounting medium with DAPI (Vectashield). Brain tumor
169 sections were imaged using an inverted Nikon TiE-PFS-A1R confocal microscope. Images were
170 post-processed using Nikon Elements software.

171 **Bone Marrow Culture**

172 Induction of MDSCs was adapted from previously published work (Alban et al.) (27). Bone marrow-
173 derived cells from wildtype C57BL/6 mice were prepared as previously described. Cells were then
174 plated at a density of 400,000 cells/cm^2 and concentration of 1,000 cells/uL in media consisting of
175 50% complete RPMI (RPMI + 10% FBS + 2mM L-Glutamine) and 50% KR158B conditioned
176 media. Additionally, the media was supplemented with 40ng/mL GM-CSF (R&D 415-ML) and
177 40ng/mL IL-6 (R&D 406-ML). On day 5, suspended cells were collected, the flask was washed in
178 PBS and scraped using a cell scraper (Fisher), and all contents were joined together in a 50mL
179 conical tube. Cells were collected via centrifugation (4 °C, 380 × *g*, 5 min) and counted by trypan
180 blue exclusion. Cells were then either subjected to flow cytometry (see "Flow Cytometry Analysis")
181 or utilized for the T cell suppression assay (see "T cell Suppression Assay").

182 **T cell Suppression Assay**

183 Following a 5-day culture (see "Bone Marrow Culture"), MDSC enriched bone marrow cells were
184 collected from culture as described above and subjected to M-MDSC magnetic bead isolation
185 (Miltenyi Biotec) according to manufacturer's protocols. Additionally, fresh splenocytes were
186 isolated as previously described and subjected to Pan-T cell magnetic bead isolation (Miltenyi
187 Biotec) according to manufacturer's protocols. Following isolation, T cells were collected via
188 centrifugation and resuspended at a density of 1million cells/mL in PBS. T cells were incubated with
189 1uL Cell Trace Far Red Cell Proliferation dye (ThermoFisher C34564) per 1 million cells for 20
190 minutes at RT. Following incubation, the dye was quenched in 5 times the present volume of
191 complete RPMI. T cells were collected via centrifugation (4 °C, 380 × *g*, 5 min) and resuspended in
192 complete RPMI at 1,000 cells/uL. Dynabeads Mouse T Activator CD3/CD28 beads (Thermofisher
193 11452D) were washed in complete RPMI and mixed with stained T cells at a 2:1 (activating bead:T
194 cell) ratio. T cells were retained at each step to ensure for unstained, unstimulated, and stained,
195 unstimulated controls. 100,000 T cells were added per well in a round-bottom 96-well plate and
196 MDSCs were added at ratios of 1:4, 1:2 and 1:1 (MDSCs:T cells). Co-cultures were incubated at
197 37°C for 3 days. Following incubation, well contents, in addition to 2 subsequent PBS well washes,
198 were transferred to centrifuge tubes. Tubes were then placed on the Dynamag-2 (Thermofisher
199 12321D) to remove activating beads. Cells were collected by centrifugation and stained for CD3,

200 CD4 and CD8 (Biolegend 100234; 100510; 100708) for flow cytometry analysis. Each biologic and
201 condition were run in triplicate. Technical triplicates were averaged prior to statistical analysis.

202 **In Vitro Cell Migration**

203 Bone marrow cells were isolated from *Ccr2$^{WT/RFP}$/Cx3cr1$^{WT/GFP}$* mice as described previously. Cells
204 were diluted to a final concentration of 2,000 cells/µL in migration buffer consisting of RPMI-1640,
205 25mM HEPES, 1% penicillin-streptomycin, and 0.1% BSA (>98% quality). In vitro migration of
206 CCR2$^{WT/RFP}$/CX3CR1$^{WT/GFP}$ cells was assessed using a transwell-96 well plate with 5uM
207 polycarbonate membrane (Corning; product number 3388). Recombinant Mouse CCL2, CCL7, and
208 soluble CX3CL1 chemokines were purchased from R & D Systems (product numbers 479-JE-010;
209 456-MC-010; 571-MF-025). Recombinant proteins were reconstituted following manufacture
210 preparation and storage guidelines. Recombinant CCL2, CCL7, and soluble CX3CL1 ligands were
211 diluted in migration buffer and seeded at 150µL/well in the bottom chamber. To validate a
212 chemotaxis effect, chemokine was also placed in the top and bottom chambers at equivalent
213 concentrations (i.e., 30ng/mL top chamber and 30ng/mL bottom chamber). Cells were plated at
214 150µL/well in the top chamber, and the plate was incubated at 37°C, 5% CO_2 for 2 hours. After
215 incubation, the membrane insert was lightly shaken to detach migrated cells on the underside of the
216 membrane and then discarded. Wells were analyzed for CCR2$^{WT/RFP}$ and CCR2$^{WT/RFP}$/CX3CR1$^{WT/GFP}$
217 populations using single color compensation on Beckman Coulter CytoFLEX LX 96-well plate
218 system. 75uL/well was collected at a flow rate of 150uL/min with 3s shake time and backflush
219 between wells. Gating strategy proceeded as follows: 1. Positive gate for myeloid population
220 according to forward-scatter area (FSC-A) and side-scatter area (SSC-A). 2. Doublet exclusion
221 according to FSC-A and forward-scatter height (FSC-H). 3. CCR2/CX3CR1 co-expression according
222 to PE and FITC channels. Gating strategy was established according to analysis of raw bone marrow
223 samples and applied constantly throughout the analysis. Final gating analysis was conducted using
224 FCS Express software (De Novo) or FlowJo V10.8.1 (BD Biosciences). Control wells containing no
225 chemokine in the bottom well were averaged and normalized as 100% migration. Sample wells are
226 compared relative to control wells for presentation and statistical analyses.

227 For analysis of migration to conditioned media, KR158B or KR158B-CCL2 KD cells were cultured
228 to 90% confluency in a tissue-culture T-75 flask containing complete DMEM (see "Cell Culture"
229 section in methods). Media was washed out and cells were plated in a 6-well plate in 6mL migration
230 buffer at 50, 100, 500 cells/µL overnight at 37 °C, 5% CO_2. Contents from wells were extracted and
231 centrifuged at 1,000 RPM for 5 minutes. Supernatant was collected, filtered, and aliquoted in the
232 bottom chamber of the transwell-96 well plate. For neutralization experiments, polyclonal goat IgG
233 antibodies (anti-CCL2, anti-CCL7, and normal goat IgG control) were purchased from R & D
234 Systems (product number AB-479-NA, AF-456-NA, and AB-108-C) and stored following
235 manufacture instructions. All wells that received neutralizing antibodies received equal quantities of
236 exogenous protein (i.e., 8.25 µg/well) through supplementation of normal goat IgG control. Raw
237 bone marrow was seeded in the top chamber as previously mentioned. Each biologic and condition
238 were run in triplicate. Technical triplicates were averaged prior to statistical analysis.

239 **Survival Analysis**

240 The complete human glioblastoma multiforme (GBM) patient dataset was mined from The Cancer
241 Genome Atlas (TCGA Research Network: cancer.gov/tcga) The Georgetown Database of Cancer (G-
242 DOC) platform to extract gene expression and clinical parameters(28–30). G-DOC platform was
243 accessed on February 4, 2022. Gene expression was gathered from the Affymetrix dataset
244 (Affymetrix HT Human Genome U133a microarray platform by the Broad Institute of MIT and

245 Harvard University cancer genomic characterization center) and RNA sequencing dataset (Illumina
246 HiSeq 2000 RNA Sequencing platform by the University of North Carolina TCGA genome
247 characterization center). Patients were stratified into low or high CCL2, CCL7, and CCL2 ∩ CCL7
248 expressing categories (LOW<25th percentile and HIGH>75th percentile, respectively). Percentiles
249 were generated using descriptive statistics function in GraphPad Prism version 9.3.1 for Windows,
250 GraphPad Software, San Diego, California USA. Survival curve comparisons and numbers at risk
251 were calculated using Log-rank (Mantel-Cox test) and graphically illustrated through GraphPad
252 Prism version 9.3.1. P-values are reported in figures.

253 **Statistical Analysis**

254 Multiple t-tests, Log-rank (Mantel-Cox), one-way ANOVA and two-way ANOVA analyses were
255 performed in GraphPad Prism version 9.3.1 to determine statistically significant differences between
256 groups. Multiple comparisons were corrected for with the recommended Dunnett multiple
257 comparison test. A p-value <0.05 was considered significant and is indicated by symbols depicted in
258 the figures, figure legends and text.

259 **Results**

260 **CCR2$^+$/CX3CR1$^+$ cells in the glioma-microenvironment are sourced from the bone marrow**

261 We previously established that a glioma-associated CCR2$^+$/CX3CR1$^+$ myeloid cell population also
262 expresses markers consistent with M-MDSCs. A CCR2$^+$/CX3CR1$^+$ myeloid cell population,
263 expressing the same MDSC markers, is also present in bone marrow. To examine the T cell
264 suppressive and migratory properties of these CCR2$^+$/CX3CR1$^+$ cells, dual transgenic
265 *Ccr2$^{WT/RFP}$/Cx3cr1$^{WT/GFP}$* mice were utilized in order to facilitate the direct examination of CCR2-
266 and CX3CR1-expressing cells. Fluorescent confocal microscopy of intracranial KR158B tumors
267 confirmed the presence of brain-resident CX3CR1$^{WT/GFP}$ microglia and revealed that CCR2$^{WT/RFP}$ and
268 CCR2$^{WT/RFP}$/CX3CR1$^{WT/GFP}$ cells were also present within the TME as early as 5 days post-
269 implantation of KR158B tumor cells (**Figure 1A**). Fluorescent imaging of naïve (non-tumor) brain
270 tissue confirmed the absence of any RFP-expressing cells in non-tumor bearing brain tissue while
271 RFP/GFP positive cells were present in bone marrow (**Figure 1A**).

272 To directly establish if CCR2$^+$/CX3CR1$^+$ cells present within KR158B gliomas are sourced from the
273 bone marrow we generated chimeric mice harboring *Ccr2$^{WT/RFP}$/Cx3cr1$^{WT/GFP}$* bone marrow cells.
274 Irradiated wild type C57BL/6 mice (recipient) received whole bone marrow isolated from
275 *Ccr2$^{WT/RFP}$/Cx3cr1$^{WT/GFP}$* mice (donor) and, following immune reconstitution, chimeric mice were
276 orthotopically implanted with KR158B glioma cells. At experimental endpoint, bone marrow and
277 brain tumor tissue were processed for flow cytometry. Flow cytometry analysis identified the
278 presence of CCR2$^+$ and CCR2$^+$/CX3CR1$^+$ cells in the tumors of chimeric mice (p<.0001) (**Figure**
279 **1B, C**) which indicates that these populations were derived from the bone marrow. GFP+ cells were
280 absent from these tumors, suggesting that this population is brain-derived.

281 **CCR2$^+$/CX3CR1$^+$ cells suppress CD8 and CD4 T cell proliferation and IFN-γ production**

282 To investigate the functionality of CCR2$^+$/CX3CR1$^+$ cells, the impact on T cell proliferation and
283 function was assessed. Having determined that CCR2$^+$/CX3CR1$^+$ cells are bone marrow-derived,
284 whole bone marrow was harvested and cells were cultured in the presence of KR158B glioma-
285 derived factors (conditioned media) containing soluble GM-CSF and IL-6 to enrich and expand the
286 population of dual-expressing chemokine receptor cells. Following magnetic bead MDSC isolation,

287 flow cytometry analysis confirmed the isolation of cells expressing CD45, CD11b, Ly6C, and
288 chemokine receptors CCR2 and CX3CR1 (**Figure 2A**); cells were negative for Ly6G. The enriched,
289 bone marrow-derived cells significantly suppressed the proliferation of both CD4$^+$ and CD8$^+$ T cells
290 at ratios 1:2 and 1:1 (**Figure 2B-D**). In the presence of MDSCs at a 1:2 ratio, CD4$^+$ T cell
291 proliferation decreased from 71% to 39% while CD8$^+$ T cell proliferation decreased from 82% to
292 50%. When co-cultured at a 1:1 ratio of MDSCs to T cells, CD4$^+$ and CD8$^+$ T cell proliferation was
293 suppressed to 20% and 18%, respectively (**Figure 2C, D*)***. To further assess suppression within the
294 co-culture, we analyzed the media from the suppression assay for levels of IFN-γ. Consistent with the
295 results for proliferation, higher ratios of MDSCs:T cells also yielded lower concentrations of IFN-γ
296 within the co-culture (**Figure 2E**), suggesting functional inhibition of effector T cells by the
297 CCR2$^+$/CX3CR1$^+$ MDSCs. These results establish that bone marrow CCR2$^+$/CX3CR1$^+$ cells, when
298 incubated in glioma-derived factors, acquire a phenotype capable of disrupting the proliferation and
299 function of both CD4- and CD8-expressing T cells.

300 **High CCL2 and CCL7 expression is associated with lower overall survival in human**
301 **glioblastoma**

302 Of the five known human ligands of CCR2, three are shared with mice, namely CCL2, CCL7 and
303 CCL8. To determine the impact of these chemokines on the clinical prognosis of human GBM, gene
304 expression and survival data from The Cancer Genome Atlas (TCGA) GBM cohort was analyzed.
305 Patients were stratified into "Low" and "High" expressing categories based on the lowest and highest
306 quartiles of expression. Kaplan-Meyer survival curves, derived from Affymetrix and
307 IlluminaHighseq datasets, were generated and Log-rank tests were utilized to compare the survival
308 distributions. Similar to findings of Chang et al., a statistically significant decrease in survival among
309 patients with high expression of CCL2, compared to low-expressing patients, was evident in the
310 Affymetrix gene expression dataset ($p<0.0005$) (**Figure 3A**)(31). Similar results based on CCL7
311 expression were identified ($p=0.0417$) (**Figure 3B**). Upon grouping cohorts of high expression of
312 CCL2 and CCL7 and low expression of CCL2 and CCL7 (denoted as the intersection sign "∩"),
313 there was a statistically significant decrease in survival among the high expression cohort ($p=0.0255$)
314 (**Figure 3C**). More striking results were revealed when analyzing the Illumina Highseq dataset. High
315 CCL2 expression ($p=0.0109$) (**Figure 3D**) and high CCL7 ($p=0.0319$) (**Figure 3E**) expression among
316 patients correlated with a statistically significant reduction in survival. This survival disadvantage
317 was most pronounced among patients with high expression of both CCL2 and CCL7 ($p=0.0018$)
318 (**Figure 3F**). These results indicate that high expression of CCL2 and CCL7 is negatively correlated
319 with survival in the context of human GBM. Expression of CCL8, the other shared CCR2 chemokine
320 across species, was not associated with a significant survival disadvantage (**Supplementary Figure**
321 **3C**). CCL13 and CCL16, CCR2 ligands found only in humans, also did not show a significant
322 survival disadvantage (**Supplementary Figure 3**). Taken together with our previous data, we posit
323 that this significant difference in survival between low and high expressors is due in part to an
324 elevated level of recruitment of immunosuppressive CCR2$^+$/CX3CR1$^+$ cells into the glioma
325 microenvironment.

326 **CCR2$^+$/CX3CR1$^+$ cells migrate to recombinant CCL2 and CCL7 through CCR2**

327 With evidence that CCR2$^+$/CX3CR1$^+$ cells represent a potent T cell suppressive population and
328 CCR2 ligands (CCL2 and CCL7) confer poor survival in human GBM, we evaluated the impact of
329 CCL2 and CCL7 on cell migration. To determine the migratory capacity of the CCR2$^+$/CX3CR1$^+$
330 cell population to chemokine ligands, a 96-well 5-uM transwell migration assay was employed.
331 Migration of CCR2$^+$/CX3CR1$^+$ cells was determined using flow cytometry, gating for CCR2$^{WT/RFP}$

332 and CX3CR1$^{WT/GFP}$ double-positive cells (**Figure 4A**) with results presented as percent migration
333 relative to the control condition i.e., no recombinant chemokine in the bottom chamber.

334 Flow cytometry analysis revealed statistically significant migration of CCR2$^+$/CX3CR1$^+$ cells to
335 recombinant CCL2 and CCL7 (**Figure 4B, C**). Cells derived from naïve animals achieved a
336 maximum percent migration to both ligands at a plating concentration of 30ng/mL ($p<0.0001$). These
337 cells displayed a higher efficacy for CCL7 relative to CCL2, achieving a mean percent migration of
338 559% and 366% to CCL7 and CCL2 respectively (**Figure 4C**). Bone marrow-derived cells from
339 tumor-bearing animals 3-week post-implantation also displayed statistically significant migration,
340 achieving maximum migration of 500% and 334% at a plating concentration of 10ng/mL and
341 30ng/mL for CCL2 and CCL7 respectively ($p<0.0001$) (**Figure 4B**). Distinct from the naïve
342 condition, cells from the tumor-bearing animal migrate to CCL2 with a slightly higher potency as
343 compared to CCL7 and achieve near-maximum migration to both ligands at as low as 3ng/mL of
344 recombinant protein plated in the bottom chamber.

345 To establish that the effect shown through these transwell migration assays was due to chemotaxis
346 (directed cell movement in response to a chemokine gradient) as opposed to increased chemokinetic
347 (random cell movement) activity, recombinant chemokine was plated at equal concentrations in both
348 chambers. Disruption of the chemokine gradient, at 30ng/mL concentrations of ligand prevented
349 migration of bone marrow cells derived from either naïve or tumor-bearing animals. (**Figure 4B, C**).
350 To determine if the migration was dependent on functional CCR2, bone marrow-derived cells from
351 tumor-bearing CCR2-deficient mice (*Ccr2$^{RFP/RFP}$*) were analyzed for CCL2-dependent migration.
352 RFP-expressing cells from the *Ccr2$^{RFP/RFP}$* mouse did not migrate to any of the CCL2 concentrations
353 tested (**Figure 4B**). This indicates that CCR2-expressing cells migrate to the chemokines CCL2 and
354 CCL7 in a CCR2-dependent mechanism. Since this cell population also expresses CX3CR1,
355 migration of bone marrow-derived cells from tumor-bearing *Ccr2$^{+/RFP}$/Cx3cr1$^{+/GFP}$* mice to soluble
356 CX3CL1 was assessed. There was no statistically significant migration of CCR2$^+$/CX3CR1$^+$ cells to
357 CX3CL1 (**Supplemental Figure 5B**). Taken together, these results suggest that bone marrow-
358 derived CCR2$^+$/CX3CR1$^+$ cells from naïve and tumor-bearing animals migrate to CCL2 and CCL7,
359 in a CCR2-dependent manner.

360 **KR158B CCL2 and CCL7 knockdown gliomas contain equivalent percentages of**
361 **CCR2$^+$/CX3CR1$^+$ MDSCs compared to KR158B gliomas**

362 To evaluate whether KR158B tumor cells are active contributors in the recruitment of
363 CCR2$^+$/CX3CR1$^+$ cells, we tested whether glioma cells produced and secreted CCL2 and CCL7.
364 ELISA analysis of the conditioned media of KR158B cells determined that after 24 hours, glioma
365 cells plated at 500 cells/uL had produced 11.1ng/mL of CCL2 and 1.9ng/mL of CCL7. Simultaneous
366 ELISA analysis of KR158B CCL2 knockdown (KR158B CCL2 KD) and KR158B CCL7
367 knockdown (KR158B CCL7 KD) cell lines revealed a statistically significant decrease in production
368 of CCL2 and CCL7, measured at 2.7ng/mL and 0.8ng/mL respectively ($p<0.0001$) (**Figure 5A, B*)***.

369 KR158B, KR158B CCL2 KD or KR158B CCL7 KD glioma cell lines were implanted in
370 *Ccr2$^{+/RFP}$/Cx3cr1$^{+/GFP}$* mice, and flow cytometry analysis of tumors and bone marrow was conducted
371 4.5 weeks post-implantation (**Figure 5C**). We found no significant differences in infiltrating
372 populations of CCR2$^+$/CX3CR1$^+$ cells, induced by KR158B CCL2 KD and KR158B CCL7 KD
373 glioma cell lines, when compared to KR158B (**Figure 5D**). We also saw no changes in the
374 population of CCR2$^+$/CX3CR1$^+$ cells in the bone marrow of mice harboring chemokine knockdown
375 gliomas (**Figure 5E*)***. These results suggest that decreased production of a single chemokine by

376 glioma cells does not impact recruitment of CCR2$^+$/CX3CR1$^+$ cells to the TME. The lack of effect
377 observed following the implantation of individual CCL2 or CCL7 knockdown gliomas suggested a
378 potential chemokine ligand redundant mechanism utilized by the KR158B cells to recruit
379 CCR2$^+$/CX3CR1$^+$ cells to the TME.

380 **CCR2$^+$/CX3CR1$^+$ cell migration to KR158B conditioned media is inhibited with CCL2 and**
381 **CCL7 neutralizing antibodies**

382 We next sought to determine whether bone marrow-derived CCR2$^+$/CX3CR1$^+$ cells migrate to
383 KR158B conditioned media. Utilizing the same transwell migration assay and flow cytometry gating
384 strategy as described above, conditioned media was plated as the chemoattractant, and migration was
385 analyzed. These results indicate that CCR2$^+$/CX3CR1$^+$ cells migrate significantly to the conditioned
386 media of both the KR158B and KR158B-CCL2 KD glioma cell lines. CCR2$^+$/CX3CR1$^+$ cells
387 migrated to the conditioned media of the KR158B cell line with a maximum percent migration of
388 266% relative to the migration buffer control condition (p=0.0006) (**Figure 6A**). Consistent with our
389 in vivo results, this cell population migrated similarly to the conditioned media of the KR158B CCL2
390 KD cell line, achieving a maximum percent migration of 242% relative to the control (p=0.004). Of
391 note, statistically significant migration was only achieved in conditions in which the conditioned
392 media of KR158B or KR158B CCL2 KD cells was derived from 24-hour cultures plated at a
393 concentration of 500cells/uL. A positive control with recombinant CCL2 at 10ng/mL as the
394 chemoattractant confirmed the migratory potential of the cells. Upon validating CCR2$^+$/CX3CR1$^+$
395 cell migration to the conditioned media of KR158B and KR158B CCL2 KD glioma cell lines, we
396 sought to determine whether the migration was exclusively mediated by CCL2 and/or CCL7. To
397 evaluate this question, we plated KR158B cells at various densities and collected the conditioned
398 media after 24 hours. The impact of anti CCL2 or anti-CCL7 neutralizing antibodies or a
399 combination of both was evaluated on migration to the KR158B conditioned media.

400 CCR2$^+$/CX3CR1$^+$ cells migrated significantly to conditioned media containing non-immune IgG
401 with a percent migration of 413% (p<0.0001) (**Figure 6B**). There was no statistically significant
402 difference observed between migration to conditioned media with or without non-immune IgG. In the
403 conditions in which conditioned media was supplemented with a low concentration of neutralizing
404 antibody (10ug/mL α-CCL2 or 1ug/mL α-CCL7), we observed no significant reduction in overall
405 migration. To determine if migration could be inhibited by supplementing with a higher neutralizing
406 antibody concentration, the conditioned media was supplemented with 50ug/mL α-CCL2 or 5ug/mL
407 α-CCL7. When supplementing with 50ug/mL α-CCL2, a significant reduction in percent migration
408 from 413% in the control condition to 240%, a 42% reduction (p=0.016) was evident. Similarly,
409 when supplementing the conditioned media with the high dose of α-CCL7, 5ug/mL, migration was
410 reduced from 413% to 192%, a 54% reduction (p=0.0015).

411 As CCR2$^+$/CX3CR1$^+$ cells migrate similarly to CCL2 and CCL7, we then assessed whether there was
412 redundancy between the chemokines that would facilitate cell migration in the event that one ligand
413 was neutralized. To evaluate this, the conditioned media was supplemented with either low
414 combinations (10ug/mL α-CCL2 and 1ug/mL α-CCL7) or high combinations (50ug/mL α-CCL2 and
415 5ug/mL α-CCL7) of neutralizing antibodies. Interestingly, supplementing with either the low or high
416 combination of neutralizing antibodies resulted in complete inhibition of migration. In the case of the
417 low neutralizing antibody combination, CCR2$^+$/CX3CR1$^+$ cells achieved 99% migration, whereas
418 cells in the high neutralizing antibody condition reached only 89% migration compared to the
419 migration buffer control normalized to 100% (p<0.0001) (**Figure 6B**).

420 To validate that CCR2 was responsible for the migration of CCR2$^+$/CX3CR1$^+$ cells to KR158B
421 conditioned media, bone marrow cells derived from a *Ccr2*-deficient mouse were utilized. Using

422 conditioned media as the chemoattractant, no statistically significant migration of RFP-expressing
423 cells to conditioned media, as compared to the buffer control, was seen (**Figure 6B**). Taken together,
424 these results show that CCR2$^+$/CX3CR1$^+$ cells migrate to CCL2 and CCL7 produced by KR158B
425 cells through CCR2, and this migration can be disrupted through pharmacologic or genetic disruption
426 of this chemokine-receptor axis.

427 **Discussion**

428 Glioblastoma is a highly aggressive disease which exhibits a significant immune suppressed tumor
429 microenvironment, lending to its poor prognosis (32–36). Although representing a diverse population
430 in itself, infiltrating myeloid cell populations contribute to the suppressed environment and promote
431 tumor growth (7,8,37–39). Our earlier studies established that CCR2$^+$/CX3CR1$^+$ myeloid cells,
432 characterized by M-MDSC markers, are present in the bone marrow and infiltrate into multiple
433 murine gliomas (KR158B and 005 GSC). Genetic and pharmacologic inhibition of CCR2 reduced the
434 presence of these cells in the TME, promoted sequestration of these cells in the bone marrow, and
435 unmasked an effect of an immune checkpoint inhibitor to slow glioma progression (26). While these
436 prior studies clearly support targeting CCR2$^+$/CX3CR1$^+$ cells as a means to treat gliomas, a greater
437 appreciation of the immune-suppressive and migratory properties of this CCR2$^+$/CX3CR1$^+$ cell
438 population is needed. Herein, we extend our published results to better understand the functionality
439 of these cells. The principal findings of this study are 1) glioma-associated CCR2$^+$/CX3CR1$^+$
440 myeloid cells are sourced from the bone marrow, 2) CCR2$^+$/CX3CR1$^+$ cells suppress both CD4$^+$ and
441 CD8$^+$ T cells, and 3) CCR2$^+$/CX3CR1$^+$ cells migrate to recombinant and glioma-produced CCL2 and
442 CCL7 in a redundant manner.

443 Brain tumors, and particularly gliomas, contain mixed populations of myeloid cells (40–44). Our
444 previous report provided a comprehensive analysis of the phenotypic markers expressed by myeloid
445 cells in the glioma microenvironment of both KR158B and 005 GSC intracranial tumors. Glioma-
446 associated myeloid cells can be distinguished by relative CD45 expression, with microglia and
447 peripherally sourced cells expressing mid and high levels of this marker, respectively (26,45). In
448 addition, forward scatter properties also distinguish microglia from peripheral tumor associated
449 macrophages. We established that bone marrow and glioma-associated CD45^{high}, CD11b$^+$,
450 Ly6C^{hi}/Ly6G$^-$ cells co-express CCR2 and CX3CR1. This bone marrow population expands in tumor
451 bearing mice and, pharmacological or genetic disruption of CCR2 promoted the sequestration of
452 these cells in the bone marrow (26). Using a chimeric mouse paradigm, we formally established that
453 the CCR2$^+$/CX3CR1$^+$ population is derived from the bone marrow. These findings suggest an
454 involvement of CCR2, upon stimulation by its ligands, in facilitating the trafficking of
455 CCR2$^+$/CX3CR1$^+$ cells from the bone marrow to the TME.

456 CCR2$^+$ M-MDSCs represent a prominent infiltrating immune suppressive cell population within
457 murine gliomas (31,46). Their elevated presence has shown to be correlated with negative prognosis
458 and poor response to prospective immunotherapy approaches such as immune-checkpoint inhibitors
459 (9,24). Data reported here establish that CCR2$^+$/CX3CR1$^+$ M-MDSCs are directly involved in
460 disrupting the proliferation and activated function of both CD4 and CD8-expressing T cells.
461 CCR2$^+$/CX3CR1$^+$ M-MDSCs suppressed both T cell populations with similar potency. These ex vivo
462 studies are consistent with our prior results where combined PD-1 and CCR2 blockade led to
463 decreased numbers of exhausted CD4 and CD8 T cells and increased IFN-γ expression within the
464 gliomas. Further studies will be necessary to better understand direct and indirect mechanisms
465 whereby CCR2$^+$/CX3CR1$^+$ M-MDSCs disrupt T cell function and dampen immune responses in the

466 context of glioma. Nonetheless, these data provide further rationale for preventing the infiltration of
467 these immunosuppressive cells into the TME.

468 CCR2 is a receptor that, among other functions, is primarily implicated in the chemotaxis of cells on
469 which it is expressed (47,48). A common feature amongst many chemokine receptors is the ability to
470 be stimulated by multiple structurally similar ligands. CCR2 is no exception with five known ligands:
471 CCL2, CCL7, CCL8, CCL13 and CCL16 (49). This feature facilitates functional redundancy in that
472 multiple ligands may induce similar downstream cellular effects upon signaling through the same
473 receptor. While CCL2 has previously been reported as the most potent inducer of CCR2$^+$ monocyte
474 migration, other CCR2 ligands are likely contributing to migration in a redundant manner to respond
475 to inflammation (50). Brait et al. reported elevated levels of CCL7, in addition to CCL2, in models of
476 ischemia reperfusion (51). These findings suggest that CCL2 and CCL7 may function in a redundant
477 manner to recruit CCR2-expressing cells to sites of inflammation. Additional studies have also
478 reported that the accumulation of myeloid cells within the CNS during inflammation is dependent
479 upon the presence of CCL2 and CCL7. In a CCL2- and CCL7-deficient mouse models, there was a
480 significant reduction in CD45$^+$/CD11b$^+$/Ly6C^{hi} cells that accumulated in the CNS; the markers that
481 characterize this population coincide with CCR2$^+$/CX3CR1$^+$ cells in the model utilized here. This
482 suggests that in addition to having functional CCR2, it is also necessary to maintain sufficient levels
483 of the cognate ligands to ultimately induce accumulation of this cell population in the CNS (52).
484 Other chemokine:chemokine receptor systems appear to have redundant roles, determined from
485 studies in murine glioma models, including CCR1 and CCR5 and their shared ligands (53,54). While
486 we report redundant roles for CCL2 and CCL7, there may be spatiotemporal regulation of CCR2-
487 expressing cells by these individual ligands. For instance, one chemokine, i.e., CCL2, might be the
488 prominent driver of CCR2$^+$/CX3CR1$^+$ cell recruitment to the tumor, while the second, i.e., CCL7, is
489 more important for homing to specific niches within tumor. Although soluble CX3CL1 did not
490 stimulate migration of the MDSCs, a role for membrane attached CX3CL1 in firm adhesion of the
491 cells to endothelium within the tumor vasculature remains a possibility (55,56). Studies aimed toward
492 determining specific CCL2-, CCL7-, and CX3CL1-expressing areas within the tumor would need to
493 be conducted to support these concepts.

494 In conclusion, we determined that CCR2 and its cognate ligands are prominent regulators of the
495 recruitment of a CCR2$^+$/CX3CR1$^+$ immune-suppressive cell to gliomas. The expression and
496 functional characterization of these chemokine receptors further defines the M-MDSC phenotype.
497 CCL2 and CCL7 are produced, at least in part, by glioma cells and our study indicates that CCL2 and
498 CCL7 function in a redundant manner to induce the migration of CCR2$^+$/CX3CR1$^+$ M-MDSCs. As
499 such, a more effective approach to limiting this population from gaining access to the TME should
500 involve antagonizing CCR2. However, given that high CCL2 and CCL7 expression is associated
501 with poorer prognosis in GBM patients, consideration of the relative expression of these two
502 chemokines may provide predictive value to a therapeutic strategy targeting this
503 chemokine:chemokine receptor axis.

504 **References**

505 1. Weller M, Cloughesy T, Perry JR, Wick W. Standards of care for treatment of recurrent
506 glioblastoma—are we there yet? Neuro-Oncology. 2013 Jan 1;15(1):4–27.

507 2. van Solinge TS, Nieland L, Chiocca EA, Broekman MLD. Advances in local therapy for
508 glioblastoma — taking the fight to the tumour. Nat Rev Neurol. 2022 Apr;18(4):221–36.

509 3. Stupp R, Mason WP, van den Bent MJ, Weller M, Fisher B, Taphoorn MJB, et al. Radiotherapy
510 plus concomitant and adjuvant temozolomide for glioblastoma. N Engl J Med. 2005 Mar
511 10;352(10):987–96.

512 4. Stupp R, Taillibert S, Kanner AA, Kesari S, Steinberg DM, Toms SA, et al. Maintenance
513 Therapy With Tumor-Treating Fields Plus Temozolomide vs Temozolomide Alone for
514 Glioblastoma: A Randomized Clinical Trial. JAMA. 2015 Dec 15;314(23):2535–43.

515 5. Stupp R, Hegi ME, Mason WP, van den Bent MJ, Taphoorn MJB, Janzer RC, et al. Effects of
516 radiotherapy with concomitant and adjuvant temozolomide versus radiotherapy alone on
517 survival in glioblastoma in a randomised phase III study: 5-year analysis of the EORTC-NCIC
518 trial. Lancet Oncol. 2009 May;10(5):459–66.

519 6. Ravi VM, Neidert N, Will P, Joseph K, Maier JP, Kückelhaus J, et al. T-cell dysfunction in the
520 glioblastoma microenvironment is mediated by myeloid cells releasing interleukin-10. Nat
521 Commun. 2022 Feb 17;13(1):925.

522 7. Wainwright DA, Balyasnikova IV, Chang AL, Ahmed AU, Moon KS, Auffinger B, et al. IDO
523 expression in brain tumors increases the recruitment of regulatory T cells and negatively
524 impacts survival. Clin Cancer Res. 2012 Nov 15;18(22):6110–21.

525 8. Wesolowska A, Kwiatkowska A, Slomnicki L, Dembinski M, Master A, Sliwa M, et al.
526 Microglia-derived TGF-beta as an important regulator of glioblastoma invasion--an inhibition
527 of TGF-beta-dependent effects by shRNA against human TGF-beta type II receptor. Oncogene.
528 2008 Feb 7;27(7):918–30.

529 9. Alban TJ, Alvarado AG, Sorensen MD, Bayik D, Volovetz J, Serbinowski E, et al. Global
530 immune fingerprinting in glioblastoma patient peripheral blood reveals immune-suppression
531 signatures associated with prognosis. JCI Insight. 2018 Nov 2;3(21):122264.

532 10. Mellman I, Coukos G, Dranoff G. Cancer immunotherapy comes of age. Nature. 2011
533 Dec;480(7378):480–9.

534 11. Waldman AD, Fritz JM, Lenardo MJ. A guide to cancer immunotherapy: from T cell basic
535 science to clinical practice. Nat Rev Immunol. 2020 Nov;20(11):651–68.

536 12. Gupta R, Mehta A, Wajapeyee N. Transcriptional determinants of cancer immunotherapy
537 response and resistance. Trends in Cancer. 2022 May 1;8(5):404–15.

538 13. Bristol Myers Squibb Announces Update on Phase 3 CheckMate -548 Trial Evaluating Patients
539 with Newly Diagnosed MGMT-Methylated Glioblastoma Multiforme [Internet]. [cited 2021
540 Nov 22]. Available from: https://news.bms.com/news/details/2020/Bristol-Myers-Squibb-

541 Announces-Update-on-Phase-3-CheckMate--548-Trial-Evaluating-Patients-with-Newly-
542 Diagnosed-MGMT-Methylated-Glioblastoma-Multiforme/default.aspx

543 14. Reardon DA, Brandes AA, Omuro A, Mulholland P, Lim M, Wick A, et al. Effect of
544 Nivolumab vs Bevacizumab in Patients With Recurrent Glioblastoma: The CheckMate 143
545 Phase 3 Randomized Clinical Trial. JAMA Oncol. 2020 Jul 1;6(7):1003–10.

546 15. Kamran N, Kadiyala P, Saxena M, Candolfi M, Li Y, Moreno-Ayala MA, et al.
547 Immunosuppressive Myeloid Cells' Blockade in the Glioma Microenvironment Enhances the
548 Efficacy of Immune-Stimulatory Gene Therapy. Molecular Therapy. 2017 Jan 4;25(1):232–48.

549 16. Kamran N, Chandran M, Lowenstein PR, Castro MG. Immature Myeloid Cells in the Tumor
550 Microenvironment: Implications for Immunotherapy. Clin Immunol. 2018 Apr;189:34–42.

551 17. Kumar R, Mooij T de, Peterson TE, Kaptzan T, Johnson AJ, Daniels DJ, et al. Modulating
552 glioma-mediated myeloid-derived suppressor cell development with sulforaphane. PLOS ONE.
553 2017 Jun 30;12(6):e0179012.

554 18. Veglia F, Sanseviero E, Gabrilovich DI. Myeloid-derived suppressor cells in the era of
555 increasing myeloid cell diversity. Nature Reviews Immunology. 2021 Feb 1;1–14.

556 19. Bronte V, Brandau S, Chen SH, Colombo MP, Frey AB, Greten TF, et al. Recommendations for
557 myeloid-derived suppressor cell nomenclature and characterization standards. Nat Commun.
558 2016 Jul 6;7(1):1–10.

559 20. Kwak T, Wang F, Deng H, Condamine T, Kumar V, Perego M, et al. Distinct Populations of
560 Immune-Suppressive Macrophages Differentiate from Monocytic Myeloid-Derived Suppressor
561 Cells in Cancer. Cell Rep. 2020 Dec 29;33(13):108571.

562 21. Dorhoi A, Du Plessis N. Monocytic Myeloid-Derived Suppressor Cells in Chronic Infections.
563 Front Immunol. 2018 Jan 4;8:1895.

564 22. Yang Y, Li C, Liu T, Dai X, Bazhin AV. Myeloid-Derived Suppressor Cells in Tumors: From
565 Mechanisms to Antigen Specificity and Microenvironmental Regulation. Front Immunol.
566 2020;11:1371.

567 23. Tcyganov EN, Hanabuchi S, Hashimoto A, Campbell D, Kar G, Slidel TW, et al. Distinct
568 mechanisms govern populations of myeloid-derived suppressor cells in chronic viral infection
569 and cancer. J Clin Invest. 2021 Aug 16;131(16):145971.

570 24. Raychaudhuri B, Rayman P, Huang P, Grabowski M, Hambardzumyan D, Finke JH, et al.
571 Myeloid derived suppressor cell infiltration of murine and human gliomas is associated with
572 reduction of tumor infiltrating lymphocytes. J Neurooncol. 2015 Apr;122(2):293–301.

573 25. Bergenfelz C, Leandersson K. The Generation and Identity of Human Myeloid-Derived
574 Suppressor Cells. Front Oncol. 2020 Feb 7;10:109.

575 26. Flores-Toro JA, Luo D, Gopinath A, Sarkisian MR, Campbell JJ, Charo IF, et al. CCR2
576 inhibition reduces tumor myeloid cells and unmasks a checkpoint inhibitor effect to slow

577 progression of resistant murine gliomas. Proc Natl Acad Sci U S A. 2020 Jan 14;117(2):1129–
578 38.

579 27. Alban TJ, Bayik D, Otvos B, Rabljenovic A, Leng L, Jia-Shiun L, et al. Glioblastoma Myeloid-
580 Derived Suppressor Cell Subsets Express Differential Macrophage Migration Inhibitory Factor
581 Receptor Profiles That Can Be Targeted to Reduce Immune Suppression. Front Immunol.
582 2020;11:1191.

583 28. Bhuvaneshwar K, Belouali A, Singh V, Johnson RM, Song L, Alaoui A, et al. G-DOC Plus - an
584 integrative bioinformatics platform for precision medicine. BMC Bioinformatics. 2016 Apr
585 30;17(1):193.

586 29. Madhavan S, Gusev Y, Harris M, Tanenbaum DM, Gauba R, Bhuvaneshwar K, et al. G-DOC: a
587 systems medicine platform for personalized oncology. Neoplasia. 2011 Sep;13(9):771–83.

588 30. Goldman MJ, Craft B, Hastie M, Repečka K, McDade F, Kamath A, et al. Visualizing and
589 interpreting cancer genomics data via the Xena platform. Nat Biotechnol. 2020 Jun;38(6):675–
590 8.

591 31. Chang AL, Miska J, Wainwright DA, Dey M, Rivetta CV, Yu D, et al. CCL2 produced by the
592 glioma microenvironment is essential for the recruitment of regulatory T cells and myeloid-
593 derived suppressor cells. Cancer Res. 2016 Oct 1;76(19):5671–82.

594 32. Hishii M, Nitta T, Ishida H, Ebato M, Kurosu A, Yagita H, et al. Human glioma-derived
595 interleukin-10 inhibits antitumor immune responses in vitro. Neurosurgery. 1995
596 Dec;37(6):1160–6; discussion 1166-1167.

597 33. Qian J, Luo F, Yang J, Liu J, Liu R, Wang L, et al. TLR2 Promotes Glioma Immune Evasion by
598 Downregulating MHC Class II Molecules in Microglia. Cancer Immunol Res. 2018
599 Oct;6(10):1220–33.

600 34. Ikushima H, Todo T, Ino Y, Takahashi M, Miyazawa K, Miyazono K. Autocrine TGF-beta
601 signaling maintains tumorigenicity of glioma-initiating cells through Sry-related HMG-box
602 factors. Cell Stem Cell. 2009 Nov 6;5(5):504–14.

603 35. Joseph JV, Balasubramaniyan V, Walenkamp A, Kruyt FAE. TGF-β as a therapeutic target in
604 high grade gliomas - promises and challenges. Biochem Pharmacol. 2013 Feb 15;85(4):478–85.

605 36. Nduom EK, Weller M, Heimberger AB. Immunosuppressive mechanisms in glioblastoma.
606 Neuro Oncol. 2015 Nov;17(Suppl 7):vii9–14.

607 37. Gabrusiewicz K, Ellert-Miklaszewska A, Lipko M, Sielska M, Frankowska M, Kaminska B.
608 Characteristics of the alternative phenotype of microglia/macrophages and its modulation in
609 experimental gliomas. PLoS One. 2011;6(8):e23902.

610 38. Avril T, Saikali S, Vauleon E, Jary A, Hamlat A, De Tayrac M, et al. Distinct effects of human
611 glioblastoma immunoregulatory molecules programmed cell death ligand-1 (PDL-1) and
612 indoleamine 2,3-dioxygenase (IDO) on tumour-specific T cell functions. J Neuroimmunol. 2010
613 Aug 25;225(1–2):22–33.

614 39. Chen Z, Hambardzumyan D. Immune Microenvironment in Glioblastoma Subtypes. Front
615 Immunol. 2018 May 8;9:1004.

616 40. Friebel E, Kapolou K, Unger S, Núñez NG, Utz S, Rushing EJ, et al. Single-Cell Mapping of
617 Human Brain Cancer Reveals Tumor-Specific Instruction of Tissue-Invading Leukocytes. Cell.
618 2020 Jun 25;181(7):1626-1642.e20.

619 41. Pombo Antunes AR, Scheyltjens I, Lodi F, Messiaen J, Antoranz A, Duerinck J, et al. Single-
620 cell profiling of myeloid cells in glioblastoma across species and disease stage reveals
621 macrophage competition and specialization. Nat Neurosci. 2021 Apr;24(4):595–610.

622 42. Yuan J, Levitin HM, Frattini V, Bush EC, Boyett DM, Samanamud J, et al. Single-cell
623 transcriptome analysis of lineage diversity in high-grade glioma. Genome Medicine. 2018 Jul
624 24;10(1):57.

625 43. Mantovani A, Marchesi F, Jaillon S, Garlanda C, Allavena P. Tumor-associated myeloid cells:
626 diversity and therapeutic targeting. Cell Mol Immunol. 2021 Mar;18(3):566–78.

627 44. Klemm F, Maas RR, Bowman RL, Kornete M, Soukup K, Nassiri S, et al. Interrogation of the
628 Microenvironmental Landscape in Brain Tumors Reveals Disease-Specific Alterations of
629 Immune Cells. Cell. 2020 Jun 25;181(7):1643-1660.e17.

630 45. Chen Z, Feng X, Herting CJ, Garcia VA, Nie K, Pong WW, et al. Cellular and molecular
631 identity of tumor-associated macrophages in glioblastoma. Cancer Res. 2017 May
632 1;77(9):2266–78.

633 46. Alghamri MS, Banerjee K, Mujeeb AA, Mauser A, Taher A, Thalla R, et al. Systemic Delivery
634 of an Adjuvant CXCR4–CXCL12 Signaling Inhibitor Encapsulated in Synthetic Protein
635 Nanoparticles for Glioma Immunotherapy. ACS Nano. 2022 Jun 28;16(6):8729–50.

636 47. Gschwandtner M, Derler R, Midwood KS. More Than Just Attractive: How CCL2 Influences
637 Myeloid Cell Behavior Beyond Chemotaxis. Front Immunol. 2019 Dec 13;10:2759.

638 48. Takacs GP, Flores-Toro JA, Harrison JK. Modulation of the chemokine/chemokine receptor
639 axis as a novel approach for glioma therapy. Pharmacology & Therapeutics. 2021 Jun
640 1;222:107790.

641 49. Proudfoot AEI. Chemokine receptors: multifaceted therapeutic targets. Nat Rev Immunol. 2002
642 Feb;2(2):106–15.

643 50. Chu HX, Arumugam TV, Gelderblom M, Magnus T, Drummond GR, Sobey CG. Role of CCR2
644 in inflammatory conditions of the central nervous system. J Cereb Blood Flow Metab. 2014
645 Sep;34(9):1425–9.

646 51. Brait VH, Rivera J, Broughton BRS, Lee S, Drummond GR, Sobey CG. Chemokine-related
647 gene expression in the brain following ischemic stroke: No role for CXCR2 in outcome. Brain
648 Research. 2011 Feb 4;1372:169–79.

649 52. Bardina SV, Michlmayr D, Hoffman KW, Obara CJ, Sum J, Charo IF, et al. Differential Roles
650 of Chemokines CCL2 and CCL7 in Monocytosis and Leukocyte Migration during West Nile
651 Virus Infection. J Immunol. 2015 Nov 1;195(9):4306–18.

652 53. Pham K, Luo D, Liu C, Harrison JK. CCL5, CCR1 and CCR5 in murine glioblastoma: immune
653 cell infiltration and survival rates are not dependent on individual expression of either CCR1 or
654 CCR5. J Neuroimmunol. 2012 May 15;246(1–2):10–7.

655 54. Dyer DP. Understanding the mechanisms that facilitate specificity, not redundancy, of
656 chemokine-mediated leukocyte recruitment. Immunology. 2020;160(4):336–44.

657 55. Umehara H, Goda S, Imai T, Nagano Y, Minami Y, Tanaka Y, et al. Fractalkine, a CX3C-
658 chemokine, functions predominantly as an adhesion molecule in monocytic cell line THP-1.
659 Immunol Cell Biol. 2001 Jun;79(3):298–302.

660 56. Ostuni MA, Hermand P, Saindoy E, Guillou N, Guellec J, Coens A, et al. CX3CL1 homo-
661 oligomerization drives cell-to-cell adherence. Sci Rep. 2020 Jun 3;10(1):9069.

662 **Figures**

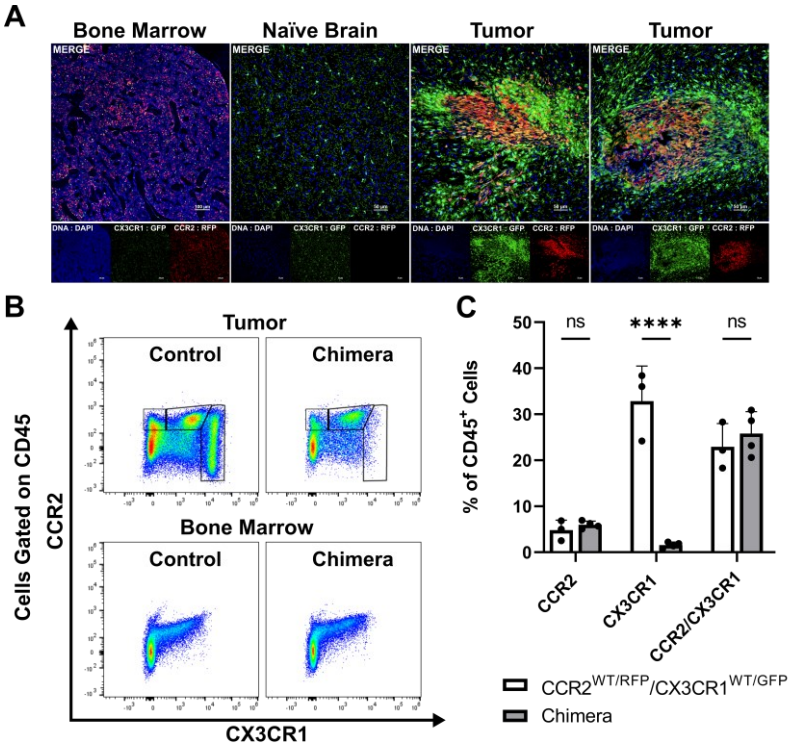

663

664 **Figure 1. CCR2/CX3CR1 cells infiltrate the glioma-microenvironment and are derived from**
665 **the bone marrow.** (**A**) Representative immunofluorescent images of naïve brain, PBS injected
666 (sham) brain, and tumor-implanted brains 5 days post implantation. Images depict the absence of
667 $CCR2^{WT/RFP}$ cells within the normal and PBS injected brain tissue and presence within tumors 5 days
668 post-implantation. (**B**) Representative flow cytometry plots of tumors and bone-marrow of non-
669 irradiated control and chimeric animals at experimental endpoint. **(C)** Quantification of $CCR2^{+}$,
670 $CX3CR1^{+}$ and $CCR2^{+}/CX3CR1^{+}$ leukocytes in control and chimeric animals. (n=3) GraphPad Prism
671 was used to conduct two-way ANOVA statistics (Dunnett's multiple comparisons test). Differences
672 are compared to the control (0) condition. p-values: 0.0332(*), 0.0021(**), 0.0002(***),
673 <0.0001(****)

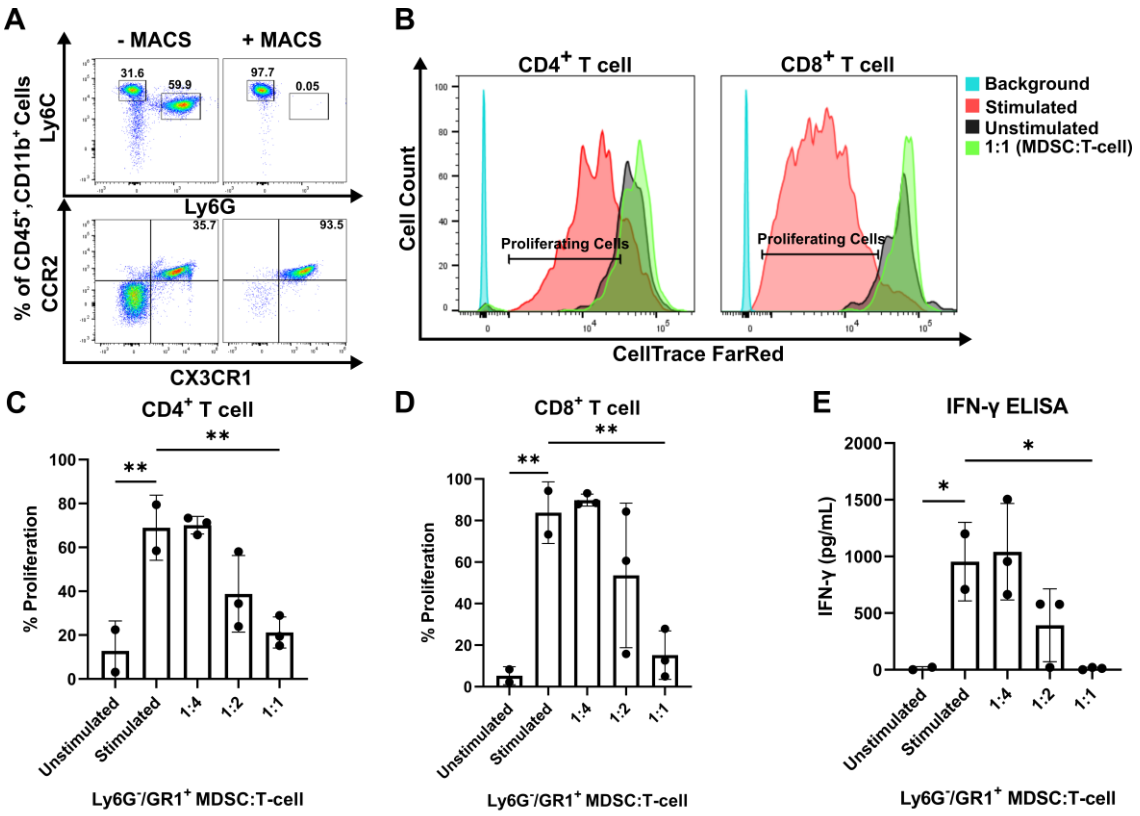

674

675 **Figure 2. CCR2+/CX3CR1+ cells suppress CD8 and CD4 T cell proliferation and IFN-γ**
676 **production. (A)** Representative flow cytometry plot establishing CCR2+/CX3CR1+ cells are
677 enriched using Ly6G and GR-1 magnetic-activated cell sorting (MACS). **(B)** Representative flow
678 cytometry plot denoting CD4+ and CD8+ proliferating cells in the presence or absence of
679 CCR2+/CX3CR1+ enriched cells. Quantification of **(C)** CD4+ or **(D)** CD8+ T cell proliferation in the
680 presence and absence of CD3/CD28 activation beads (stimulated/unstimulated) and stimulated T
681 cells co-cultured with enriched CCR2+/CX3CR1+ cells. Enriched CCR2+/CX3CR1+ cells were plated
682 at varying ratios to dye-loaded T cells (T cell numbers were held constant). After 3 days,
683 proliferation was assessed using flow cytometry (n=3). **(E)** Supernatant from co-culture T cell
684 suppression assay was collected and analyzed for IFN- γ protein via ELISA (n=3). One-way
685 ANOVA statistical analysis was conducted (Dunnett's multiple comparisons test). Differences are
686 compared to the stimulated control condition. p-values: 0.0332(*), 0.0021(**), 0.0002(***),
687 <0.0001(****)

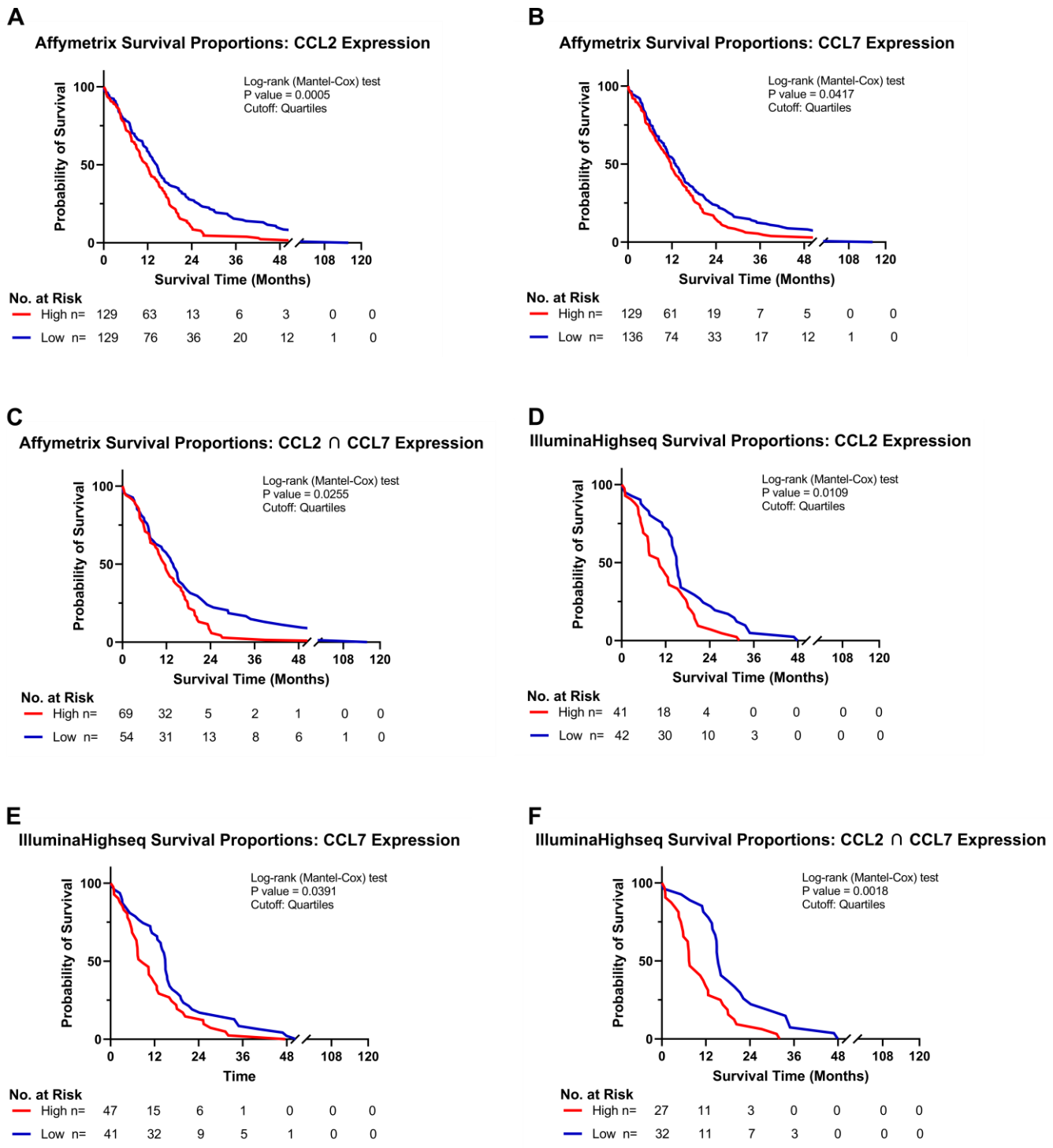

Figure 3. High CCL2 and CCL7 expression is associated with negative prognosis for patients with glioblastoma. (A-C) Kaplan-Meyer survival curves of GBM patients based on Affymetrix gene expression profiles of **(A)** CCL2 **(B)** CCL7 **(C)** intersection of CCL2 and CCL7 from TCGA database. **(D-F)** Kaplan-Meyer survival curves of GBM patients based on Illumina Highseq expression profiles of **(D)** CCL2 **(E)** CCL7 **(F)** intersection of CCL2 and CCL7 mined from TCGA database. High and low cohorts are stratified as top and bottom quartiles, respectively. Number at risk indicates surviving patients in each cohort at the respective timepoints of analysis. Log-rank (Mantel-Cox) test was conducted on high vs low expressing cohorts.

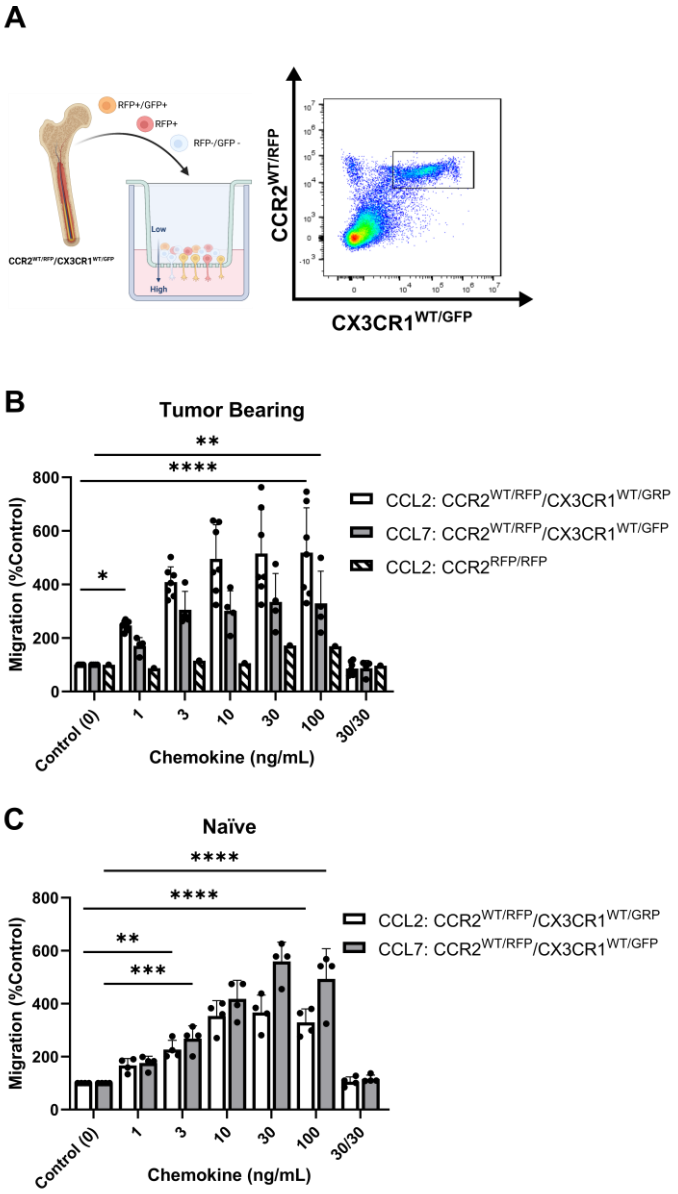

Figure 4. Bone marrow-derived CCR2+/CX3CR1+ cells migrate to recombinant CCL2 and CCL7 through CCR2. (A) Experimental design of transwell migration assays. (left) Graphic (Created with BioRender.com) depicting assay preparation in which whole bone-marrow is plated in the top chamber of the transwell migration plate. The bottom chamber contains either recombinant chemokine protein or conditioned media. (right) Representative flow plot depicting the population of CCR2+/CX3CR1+ cells quantified. **(B)** Migration to recombinant CCL2 (n=7) and CCL7 (n=4) of CCR2+/CX3CR1+ cells derived from tumor-bearing animals. Graph also depicts no migration to recombinant CCL2 of bone marrow-derived RFP-expressing cells from a Ccr2RFP/RFP animals. **(C)** Migration to recombinant CCL2 and CCL7 of CCR2/CX3CR1 expressing cells derived from naïve animals. (n=4) A condition in which chemokine was also plated in the top chamber of the transwell plate (30/30) is included to validate that migration is due to chemotaxis rather than chemokinesis. Two-way ANOVA statistical analysis was conducted (Dunnett's multiple comparisons test). Differences are compared to the control (0) condition. p-values: 0.0332(*), 0.0021(**), 0.0002(***), <0.0001(****)

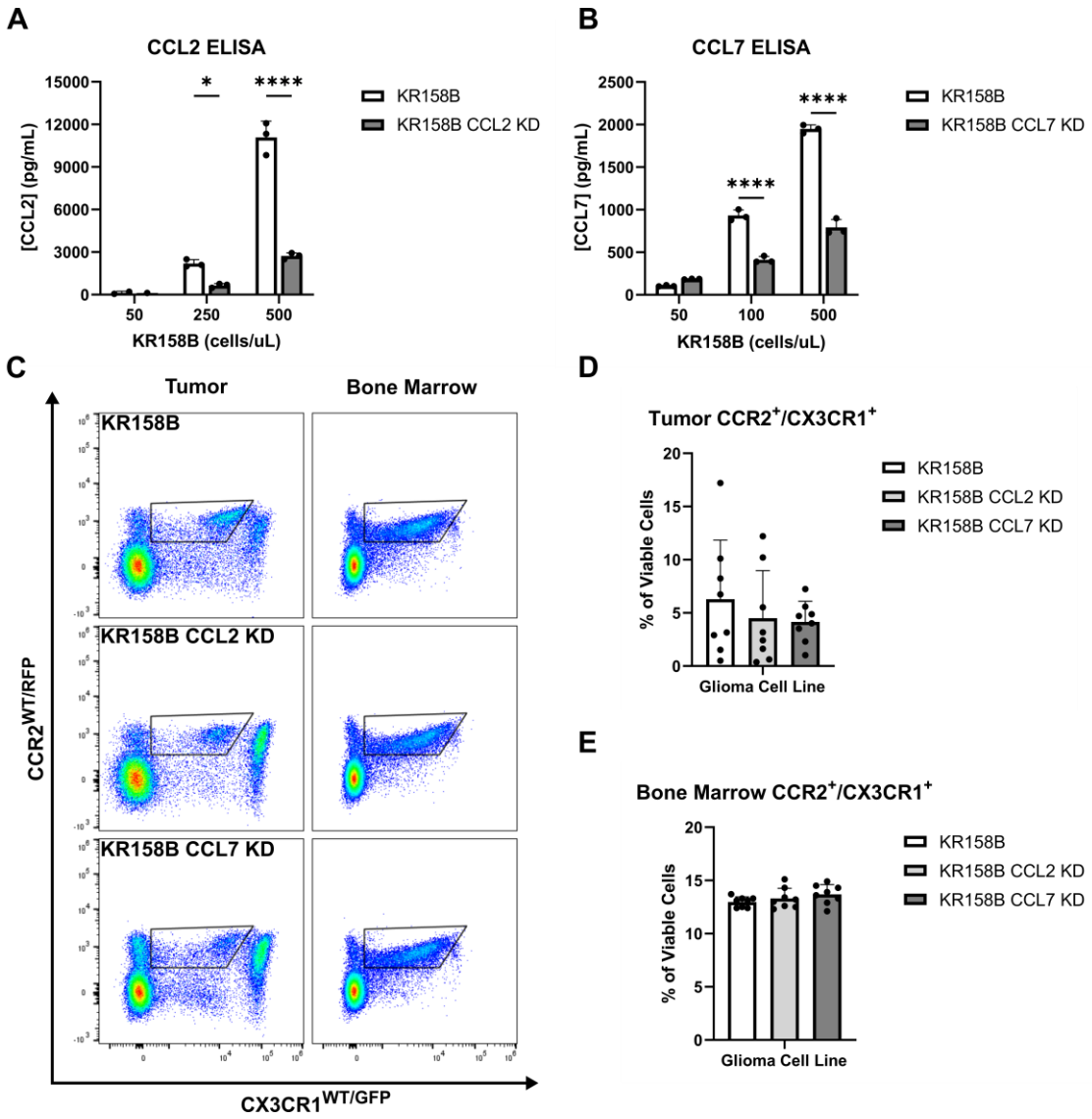

Figure 5. Infiltration of CCR2$^+$/CX3CR1$^+$ cells into tumors is equivalent in mice implanted with KR158B, KR158B CCL2 KD, or KR158B CCL7 KD tumors. (A-B) ELISA results confirming the production of **(A)** CCL2 and **(B)** CCL7 respectively from the KR158B and respective KR158B-chemokine knockdown glioma cell lines. **(C)** Representative flow plots depicting equivalent populations of CCR2/CX3CR1-expressing cells in the chemokine knockdown tumors compared to the KR158B tumor. No significant change in this population was observed in the bone marrow. **(D-E)** Graphs depicting the percent of CCR2/CX3CR1-expressing cells in the tumors and bone marrow of mice implanted with KR158B, KR158B CCL2 KD or KR158B CCL7 KD cell lines. (n=8) Two-way ANOVA statistical analysis was conducted (Dunnett's multiple comparisons test). p-values: 0.0332(*), 0.0021(**), 0.0002(***), <0.0001(****)

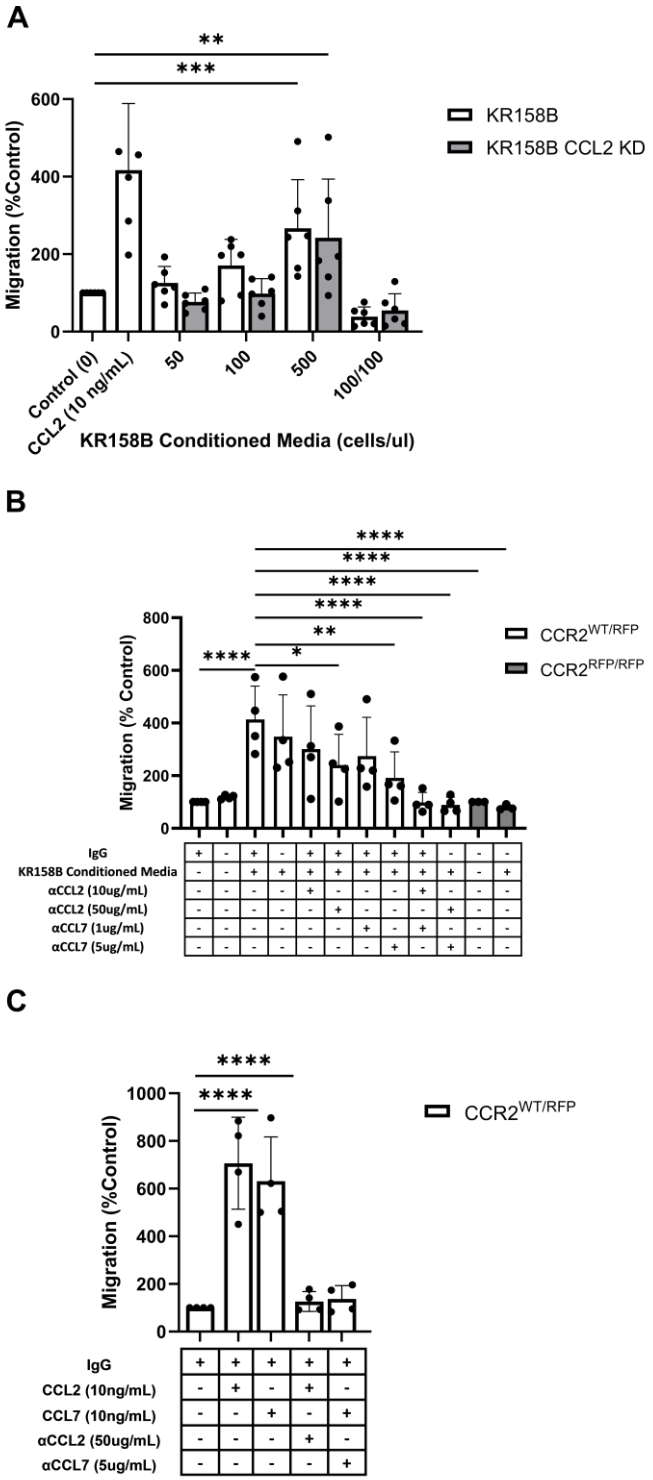

723

724 **Figure 6. Glioma-derived CCL2 or CCL7 is necessary and sufficient for bone marrow derived**
725 **CCR2/CX3CR1 cell migration. (A)** Graph depicting CCR2+/CX3CR1+ cells migrating to
726 conditioned media of KR158B (n=6) and KR158B-CCL2 knockdown (n=6) cells. A condition in
727 which conditioned media was also plated in the top chamber of the transwell plate (100/100) is
728 included to validate that migration is due to chemotaxis rather than chemokinesis. **(B)** Migration of
729 CCR2+/CX3CR1+ cells to conditioned media in the presence or absence of chemokine- neutralizing
730 antibodies. Migration is disrupted with the addition of high concentrations of single neutralizing

antibody. Migration is completely inhibited with a combination of neutralizing antibodies at either low or high concentrations. (n=4) No migration was observed to conditioned media of bone marrow-derived RFP-expressing cells from Ccr2RFP/RFP animals. (n=3) **(C)** Graph depicting that migration to exogenous recombinant CCL2 or CCL7 is inhibited through the addition of high concentrations of respective neutralizing antibody (n=4). Two-way ANOVA statistical analysis was conducted (Dunnett's multiple comparisons test). Differences are compared to the control condition or between cell lines. p-values: 0.0332(*), 0.0021(**), 0.0002(***), <0.0001(****)

Conflict of Interest

The authors declare that the research was conducted in the absence of any commercial or financial relationships that could be construed as a potential conflict of interest.

Author Contributions

GPT and CJK-designed the study, performed experiments, data analysis, data interpretation, and wrote the manuscript. DL, JSG-performed experiments. GT-performed experiments, data analysis. LPD-designed the study, data interpretation, and wrote the manuscript. DAM-designed the study, data interpretation, and wrote the manuscript. JKH-designed the study, data interpretation, and wrote the manuscript.

Funding

Research reported in this publication was supported by National Institute of Health grant RO1 NS108781 (to JKH and DAM), Florida Center for Brain Tumor Research (to JKH), as well as the National Center for Advancing Translational Sciences of the National Institutes of Health under University of Florida Clinical and Translational Science Awards TL1TR001428 and UL1TR001427 (to GPT).

Acknowledgments

We thank Joseph Flores-Toro for providing insight and technical assistance in generating chimeric mice and flow cytometry. Members of Jeffrey Martens' lab for access and training on Nikon Confocal Microscope. We gratefully acknowledge the University of Florida Interdisciplinary Center for Biotechnology Research Flow Cytometry Core and University of Florida Animal Care Service.